

Multistability of graphene nanobubbles

Alexander V. Savin^{1,2,*}

¹ N.N. Semenov Federal Research Center for Chemical Physics of the Russian Academy of Sciences, 4 Kosygin St., Moscow 119991, Russia

² Plekhanov Russian University of Economics, 36 Stremskaya Lane, Moscow 117997, Russia

Using the example of Ar, Kr, and Xe atoms, it is shown that graphene nanobubbles on flat substrates are multistable systems. A nanobubble can have many stable stationary states, each characterized by the number of layers, l , within the cluster of internal atoms. The layers are circular in shape, concentrically stacked on top of each other, forming an l -stepped pyramid with a flat top. The covering of this pyramid with a graphene sheet is achieved through its local stretching. The valence bonds of the sheet stretch only over the group of internal atoms; outside the coverage zone, the sheet remains undeformed and lies flush against the substrate. The maximum possible number of layers, l_m , increases monotonically with the number of atoms N ($l_m = 6$ for $N = 4000$). The graphene sheet, interacting with the substrate, compresses the internal atom cluster against it, generating an internal pressure of $P \sim 1$ GPa. Numerical simulations of thermal vibrations reveal that among all l -layer configurations of a nanobubble, there is always one "ground" state. Upon heating, this ground state smoothly transitions into a layerless liquid state. All other stationary states transform into this ground state once a certain temperature is reached (for $N = 4000$, the ground state corresponds to state with $l = 4$). The coexistence of several stable states with different numbers of layers at low temperatures leads to the absence of a universal shape for the nanobubbles. In this scenario, the height-to-radius ratio, H/R , can vary from 0 to 0.24, depending on the number of layers.

Keywords: Van der Waals bubble, graphene nanobubble, molecular modelling, phase transition

I. INTRODUCTION

Carbon atoms can form numerous structures, among which the monoatomic crystalline layer graphene has recently attracted significant research attention [1–5]. This nanomaterial is of great interest due to its unique electronic [6], mechanical [7], and thermal properties [8, 9]. Another important physical and chemical property of graphene is its ability to trap gas molecules under high pressure when placed on various flat substrates. This can lead to the formation of bubbles ranging in size from nanometers to micrometers.

High interest is also directed towards other graphene-like materials, such as sheets of hexagonal boron nitride (h-BN), fluorographene (CF), molybdenum disulfide (MoS₂), and tungsten selenide (WSe₂). These two-dimensional materials offer vast possibilities for creating heterostructures in the form of van der Waals stacks, which possess novel properties [10–13]. An important feature of such heterostructures is their ability to trap molecules in localized regions between adjacent layers. Due to van der Waals interactions between the layers, internal pressure on the order of several GPa can arise within these traps (nanopockets) [14–16], which can significantly change the properties of the captured material. Covering a molecular system on a flat substrate with a graphene sheet (van der Waals encapsulation) is a conve-

nient method for creating high local pressure to modify the system's properties [17] or for its storage [18–20]. In graphene nanobubbles, high pressure is induced by the forces of interaction between the sheet and the substrate.

Encapsulation structures (nanobubbles) can form spontaneously as surface defects during the mechanical transfer of two-dimensional sheets in the creation of van der Waals heterostructures [15, 21]. Nanobubbles can also be intentionally fabricated using ion bombardment [22–24] or selective adsorption methods [25].

In addition to experimental methods, analytical models and numerical simulations are used to study nanobubbles. Analytical models employ elastic plate theory, taking into account the contribution of adhesion energy between the layers of van der Waals heterostructures [26–28]. More complex models also incorporate the equation of state of the substance inside the nanobubble [29–32] and nonlinear effects [33]. Using such models, it has been shown that nanobubbles with a circular shape exhibit universal scaling behavior: the ratio of the nanobubble's height to its radius, H/R , remains constant. Numerical simulations allow not only for the verification of analytical results but also for gaining deeper insights into nanobubble properties. It has been demonstrated that spatial confinement and internal pressure within a nanobubble promote the formation of internal crystalline structures, which can be planar in shape [34], and that the nanobubble's shape can critically depend on the properties of the encapsulated substance [35]. Numerical simulations have shown [36] that a nanobubble containing an ideal gas always has a circular shape with a constant ratio $H/R = 0.204$. Molecular dynamics simula-

*Electronic address: asavin@chph.ras.ru

tions have modeled transitions of argon inside a nanobubble into a liquid-crystal state [37]. It has been demonstrated that the presence of nanobubbles can lead to a reduction in the interfacial thermal conductivity of layered van der Waals structures [38], as well as cause their significant thermal contraction [39].

In the paper, all possible stationary states of graphene nanobubbles will be numerically modeled. This paper is organized as follows. Section II describes the model used. Section III presents the possible stationary states of the nanobubbles. The stability of these stationary states against thermal fluctuations is analyzed in Section IV. The main results are summarized in the Conclusion (Section V).

II. MODEL

Let us consider a two-component molecular system consisting of a graphene sheet lying on a flat substrate and atoms of inert gas placed between them. Let the sheet comprise N_c carbon atoms, and the gas component— N_g argon (krypton, xenon) atoms. As the substrate, we will use an attractive plane at $z = 0$, corresponding to the flat surface of a silicon oxide crystal. This molecular system, consisting of $N = N_c + N_g$ atoms, represents the simplest model of van der Waals encapsulation.

Consider a rectangular graphene sheet in which the chains of valent bonds along the x -axis have a "zigzag" structure with N_x nodes, and along the y -axis—an "armchair" structure with N_y nodes (the sheet lies parallel to the $z = 0$ plane). Let us take a sheet with free edges—see Fig. 1. The sheet consists of $N_c = N_x N_y / 2 - 2$ carbon atoms and has a rectangular shape of size $L_x \times L_y$, where its length is $L_x = (N_x - 1)r_c\sqrt{3}/2$ and its width is $L_y = (3N_y/4 - 1)r_c$ ($r_c = 1.418$ Å is the C–C bond length). In all calculations, we will use a graphene sheet with $N_x = 416$, $N_y = 480$ (sheet dimensions: 50.963×50.906 nm 2 , number of carbon atoms $N_c = 99838$). We will assume that hydrogen atoms are attached to the edge carbon atoms, which participate in the formation of only two C–C bonds, forming united CH atoms with them of mass $M_e = 13m_p$ (the mass of the internal sheet atoms is $M_c = 12m_p$, where $m_p = 1.66 \times 10^{-27}$ kg is the proton mass).

The Hamiltonian of the nanosheet is

$$\mathcal{H}_1 = \sum_{n=1}^{N_c} \left[\frac{1}{2} M_c (\dot{\mathbf{u}}_n, \dot{\mathbf{u}}_n) + Q_n + Z(\mathbf{u}_n) \right], \quad (1)$$

where the vector $\mathbf{u}_n = (x_n(t), y_n(t), z_n(t))$ defines the coordinates of the n -th carbon atom at time t . The first term of the sum in equation (1) represents the kinetic energy, while the second term Q_n describes the valence interaction of the atom with index n with other atoms in the graphene sheet. This includes deformations of valence bonds, valence angles, and torsion angles—a de-

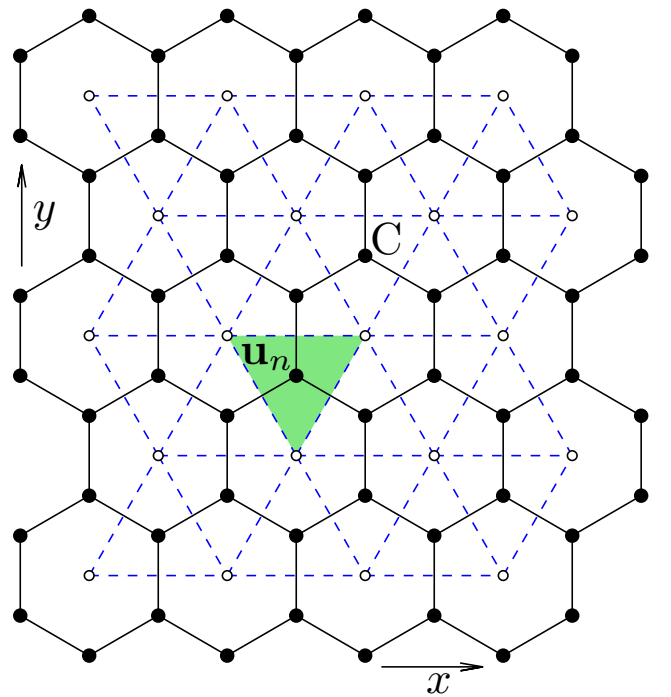


FIG. 1: A rectangular graphene sheet with $N_x = 10$, $N_y = 12$. Black disks represent carbon atoms C, black solid lines represent valence bonds C–C. Small light disks indicate the positions of the centers of mass of the valence bond hexagons. Dashed lines illustrate the triangulation of the graphene sheet using these centers—the inner surface of the sheet is divided into triangles, each containing one carbon atom (the triangle corresponding to the n -th atom is highlighted; \mathbf{u}_n is the coordinate vector of the atom).

tailed description of the force field used is provided in [40].

The valence bond between two neighboring carbon atoms n and k can be described by the Morse potential

$$U_1(\mathbf{u}_n, \mathbf{u}_k) = \epsilon_c \{ \exp[-\alpha(r_{nk} - r_c)] - 1 \}^2, \quad (2)$$

where $r_{nk} = |\mathbf{u}_n - \mathbf{u}_k|$ is the distance between the atoms, and the bond energy is $\epsilon_c = 4.9632$ eV.

Valence angle deformation energy between three adjacent carbon atoms n , k , and l can be described by the potential

$$U_2(\mathbf{u}_n, \mathbf{u}_k, \mathbf{u}_l) = \epsilon_\varphi (\cos \varphi - \cos \varphi_0)^2, \quad (3)$$

where $\cos \varphi = (\mathbf{u}_n - \mathbf{u}_k, \mathbf{u}_l - \mathbf{u}_k) / r_{nk} r_{kl}$, and $\varphi_0 = 2\pi/3$ is the equilibrium valent angle. Parameters $\alpha = 1.7889$ nm $^{-1}$ and $\epsilon_\varphi = 1.3143$ eV can be found from the small amplitude oscillations spectrum of the graphene sheet [41].

Valence bonds between four adjacent carbon atoms n , m , k , and l constitute torsion angles, the potential energy of which can be defined as

$$U_3(\mathbf{u}_n, \mathbf{u}_m, \mathbf{u}_k, \mathbf{u}_l) = \epsilon_\phi (1 - \cos \phi), \quad (4)$$

TABLE I: Values of the parameters of the interaction potential with a flat substrate (5) for atoms C, Ar, Kr, Xe.

	C	Ar	Kr	Xe
ε_0 (eV)	0.074	0.1406	0.17242	0.19462
h_0 (Å)	5.0	5.0	5.116	5.397

where ϕ is the corresponding torsion angle ($\phi = 0$ is the equilibrium value of the angle) and $\epsilon_\phi = 0.499$ eV.

The last term in the sum (1) describes the interaction of the sheet atoms with the flat substrate on which it rests. Let the flat substrate occupy the half-space $z \leq 0$. In this case, the interaction energy of a carbon atom with the substrate can be described using a (3,9) Lennard-Jones potential [42–44]:

$$Z(\mathbf{u}) = Z(z) = \varepsilon_0 \left[(h_0/z)^9 - 3(h_0/z)^3 \right] / 2, \quad (5)$$

where ε_0 is the interaction energy (adhesion energy) and h_0 is the equilibrium distance to the surface of the half-space. For a silicon dioxide (SiO_2) substrate, the energy is $\varepsilon_0 = 0.074$ eV and the distance is $h_0 = 5$ Å [45].

The Hamiltonian of the inert gas molecular subsystem has the form

$$\mathcal{H}_2 = \sum_{n=N_c+1}^N \left[\frac{1}{2} M_g (\dot{\mathbf{u}}_n, \dot{\mathbf{u}}_n) + Z(\mathbf{u}_n) \right] + E_2, \quad (6)$$

where $N = N_c + N_g$ is the total number of atoms in the two-component molecular system, the vectors $\{\mathbf{u}_n\}_{n=N_c+1}^N$ specify the coordinates of the gas atoms, and M_g is the atomic mass ($M_g = 39.96, 83.80, 131.29$ m_p for Ar, Kr, and Xe atoms, respectively). The first term in the sum (6) represents the kinetic energy of the gas subsystem, the second term—the interaction energy of the gas atoms with the flat substrate (the values of the interaction potential parameters (5) for the gas atoms are given in Table I). The last term,

$$E_2 = \sum_{n=N_c+1}^{N-1} \sum_{k=n+1}^N V(r_{nk}), \quad (7)$$

defines the interaction energy between the gas atoms, where $r_{nk} = |\mathbf{u}_n - \mathbf{u}_k|$ is the distance between atoms n and k . The interaction between atoms is described by the Lennard-Jones (6,12) potential:

$$V(r) = 4\epsilon [(\sigma/r)^{12} - (\sigma/r)^6]. \quad (8)$$

The values of the interaction potential parameters for various pairs of atoms are given in Table II.

The interaction energy between the gas atoms and the graphene sheet is given by the sum

$$E_3 = \sum_{n=1}^{N_c} \sum_{k=N_c+1}^N V(r_{nk}). \quad (9)$$

TABLE II: Values of the interaction potential parameters (8) for pairs of atoms CAr, CKr, CXe, ArAr, KrKr, XeXe [34, 46, 47].

	CAr	CKr	CXe	ArAr	KrKr	XeXe
ε_1 (eV)	0.00525	0.00643	0.00724	0.010	0.015	0.019
σ (Å)	3.3965	3.4965	3.7465	3.40	3.60	4.10

The total Hamiltonian of the two-component molecular system is

$$\mathcal{H} = \mathcal{H}_1 + \mathcal{H}_2 + E_3. \quad (10)$$

The potential energy of the molecular system is

$$E = \sum_{n=1}^{N_c} Q_n + \sum_{n=1}^N Z(\mathbf{u}_n) + E_2 + E_3. \quad (11)$$

More detailed discussion and motivation of our choice of the interaction potentials (2), (3), (4) can be found in [40]. Note that in molecular dynamics of carbon nanotubes and nanoribbons, more complex reactive potentials are often used, such as Tersoff [48], REBO [49, 50] and ReaxFF [51]. These potentials are able to describe the formation and breaking of bonds between carbon atoms, but they are worse in describing the frequency spectrum of graphene and are more complicated for numerical modeling. The use of these potentials is justified only when modeling processes in graphene-based systems that occur with changes in the topology of the valence bond lattice. Nevertheless, these potentials reliably enough describe elastic properties of graphene [52], so the decision on use them will lead to the same results.

III. STATIONARY STATES OF GRAPHENE NANOBUBBLES

To find a stationary state of an encapsulated molecular system (nanobubble), it is necessary to numerically solve the potential energy minimization problem

$$E \rightarrow \min : \{\mathbf{u}_n\}_{n=1}^N. \quad (12)$$

The problem (12) was solved numerically using the conjugate gradient method [53, 54].

As initial configurations, structures in the form of an l -layer stepped pyramid of gas atoms ($l = 1, 2, \dots$) covered from above by a graphene sheet were used. By varying the initial configuration, all possible stable stationary states of the encapsulated molecular system can be obtained.

Let $\{\mathbf{u}_n^0 = (x_n^0, y_n^0, z_n^0)\}_{n=1}^N$ be a solution to problem (12). The corresponding stationary state is characterized by its energy $E(\{\mathbf{u}_n^0\}_{n=1}^N)$, the maximum value of the vertical displacements of the graphene sheet over the

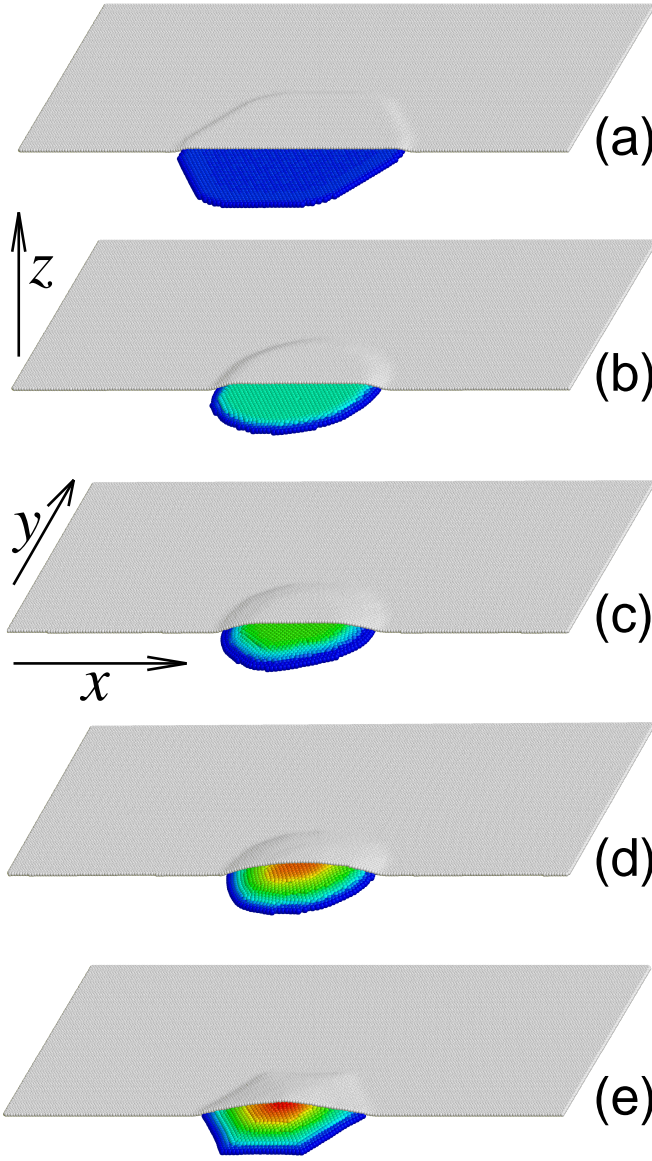


FIG. 2: Stationary l -layer states of encapsulated $N_g = 2909$ argon atoms with $l = 1$ (a), 2 (b), 3 (c), 4 (d), and 5 (e). For clarity of presentation, only one half of the graphene sheet is shown. The graphene sheet is depicted in gray. For argon atoms, their vertical displacement is indicated by color (blue corresponds to the minimum displacement with coordinate $z = h_0$, red corresponds to the maximum displacement with $z = h_0 + 10$ Å).

encapsulated group of atoms (the height of the graphene bulge)

$$H = \max_{n=1, \dots, N_c} (z_n^0 - h_0),$$

the radius R of the bulge boundary, as well as the density d and pressure P inside the nanobubble.

We will consider that a sheet atom participates in forming the upper surface of the nanobubble if its vertical displacement $\Delta z_n = z_n^0 - h_0 > h_1$, where the dis-

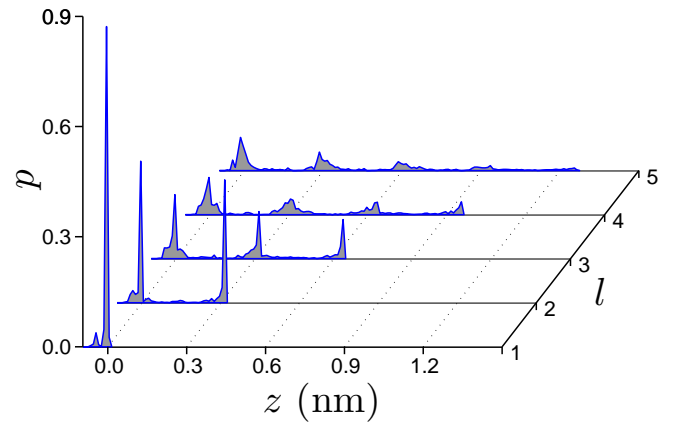


FIG. 3: Distribution of vertical displacements $p(z)$ for the stationary states of encapsulated $N_g = 3936$ krypton atoms with number of layers $l = 1, \dots, 5$.

placement threshold is $h_1 = 1.5$ Å. The center of the nanobubble then has coordinates

$$x_c = \frac{1}{N_i} \sum_{\substack{n=1 \\ \Delta z_n > h_1}}^{N_c} x_n^0, \quad y_c = \frac{1}{N_i} \sum_{\substack{n=1 \\ \Delta z_n > h_1}}^{N_c} y_n^0,$$

where the number of graphene sheet atoms forming the upper surface of the bubble is

$$N_i = \sum_{\substack{n=1 \\ \Delta z_n > h_1}}^{N_c} 1.$$

It is convenient to define the base radius of the bubble as

$$R = \frac{1}{N_r} \sum_{\substack{n=1 \\ \Delta z_n \in [h_1, h_2]}}^{N_c} r_n, \quad N_r = \sum_{\substack{n=1 \\ \Delta z_n \in [h_1, h_2]}}^{N_c} 1.$$

Here, the second vertical displacement threshold is $h_2 = 2.5$ Å, and the distance to the center is $r_n = [(x_n^0 - x_c)^2 + (y_n^0 - y_c)^2]^{1/2}$.

The volume of the encapsulation cavity beneath the graphene sheet (the nanobubble volume) is

$$V = \sum_{n=1}^{N_c} \Delta z_n S_n^0,$$

where S_n^0 is the area of the projection onto the plane $z = 0$ of the triangle corresponding to the n -th sheet atom (see the graphene sheet triangulation scheme in Fig. 1). The density of gas atoms inside the nanobubble is $d = M_g N_g / V$.

In the stationary state, a force acts on the n -th atom of the graphene sheet from the side of the encapsulated atoms:

$$\mathbf{F}_n = \frac{4\epsilon_0}{\sigma^2} \sum_{k=N_c+1}^N [2(\sigma/r_{nk})^{14} - (\sigma/r_{nk})^8] (\mathbf{u}_n^0 - \mathbf{u}_k^0),$$

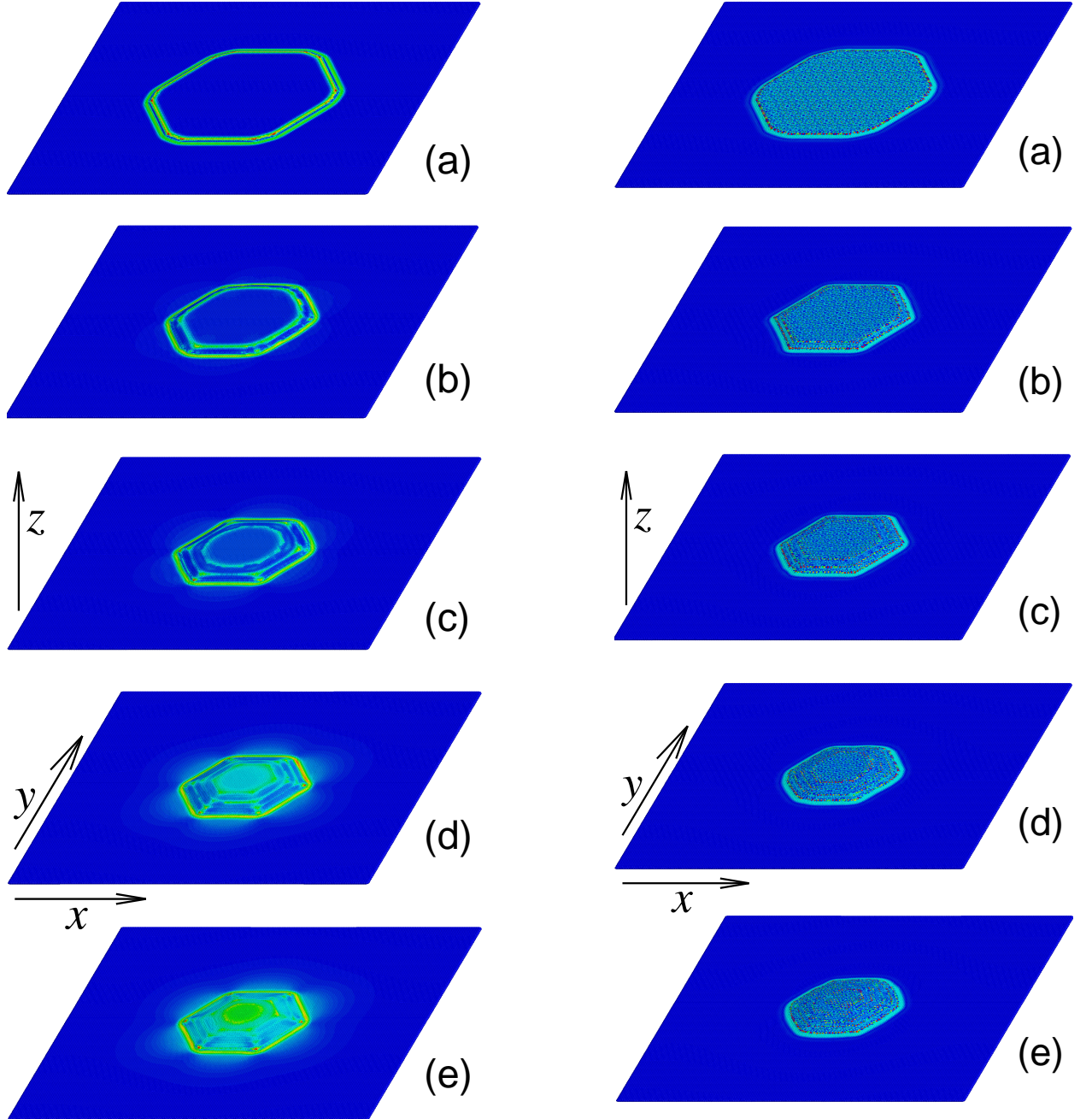


FIG. 4: Stationary l -layer states of a nanobubble with $N_g = 3936$ krypton atoms at $l = 1$ (a), 2 (b), 3 (c), 4 (d), and 5 (e). A top view is shown. Color indicates the distribution of deformation energy across the graphene sheet (blue corresponds to zero deformation, red corresponds to deformation with an energy of 0.008 eV per atom).

where the distance between atoms is $r_{nk} = |\mathbf{u}_n^0 - \mathbf{u}_k^0|$. Consequently, the local pressure on this atom is $p_n = (\mathbf{F}_n, \mathbf{e}_n)/S_n$, where \mathbf{e}_n is the unit vector orthogonal to the plane of the triangle containing the sheet atom, and S_n is the area of this triangle (see Fig. 1). The value of the average pressure on the external surface of the

FIG. 5: Stationary l -layer states of a nanobubble with $N_g = 2909$ xenon atoms at $l = 1$ (a), 2 (b), 3 (c), 4 (d), and 5 (e). A top view is shown. Color indicates the distribution of pressure across the graphene sheet (blue corresponds to zero pressure, red corresponds to a pressure of $p_n = 5$ GPa). The average pressure values are $P = 1.09, 0.90, 0.86, 0.84$, and 0.85 GPa.

nanobubble is

$$P = \frac{1}{N_i} \sum_{\substack{n=1 \\ \Delta z_n > h_1}}^{N_c} p_n.$$

This value also determines the average value of the inter-

TABLE III: Dependence on the number of encapsulated argon atoms N_g and the number of layers l of the relative specific energy ΔE , pressure P , height H , radius R , and density d of the stationary state of the nanobubble. Values for the ground states are highlighted in italics.

N_g	l	ΔE (eV)	P (GPa)	H (Å)	R (Å)	d (g/cm ³)	H/R
188	1	0	1.428	3.23	25.33	1.70	0.128
	2	0.0188	1.307	5.90	22.98	1.64	0.128
260	1	0	1.257	3.23	29.84	1.76	0.108
	2	0.0137	1.302	6.12	26.33	1.68	0.232
398	1	0	1.171	3.23	36.71	1.80	0.088
	2	0.0063	1.149	6.23	31.38	1.74	0.199
614	1	0	1.080	3.23	45.71	1.85	0.071
	2	0.0015	1.030	6.22	37.64	1.79	0.165
962	1	0	1.012	3.23	57.33	1.87	0.056
	2	-0.0018	0.950	6.22	46.57	1.82	0.165
	3	0.0010	0.953	9.11	44.30	1.79	0.206
1335	1	0	0.974	3.23	67.34	1.90	0.048
	2	-0.0046	0.866	6.22	53.08	1.85	0.117
	3	-0.0046	0.892	9.24	50.68	1.80	0.183
1828	1	0	0.942	3.23	78.83	1.91	0.041
	2	-0.0063	0.801	6.22	61.26	1.87	0.102
	3	-0.0048	0.793	9.23	56.41	1.83	0.164
	4	-0.0003	0.796	12.02	54.32	1.81	0.221
2909	1	0	0.906	3.24	99.46	1.93	0.033
	2	-0.0083	0.741	6.23	75.84	1.89	0.082
	3	-0.0063	0.767	9.25	73.10	1.85	0.127
	4	-0.0065	0.708	12.20	66.67	1.83	0.183
	5	-0.0032	0.705	14.55	64.18	1.82	0.227
3936	1	0	0.885	3.24	115.70	1.94	0.028
	2	-0.0084	0.723	6.24	88.75	1.90	0.070
	3	-0.0084	0.723	9.24	82.77	1.86	0.112
	4	-0.0097	0.696	12.24	76.09	1.84	0.161
	5	-0.0079	0.678	15.02	73.79	1.83	0.204

nal pressure.

The solution of problem (12) showed that each stationary state of a nanobubble always has a strictly defined number of atomic layers, l , in the cluster of internal atoms—see Figs. 2 and 3. For a number of encapsulated atoms $N_g < 4000$, stationary states with $l = 1, \dots, 6$ layers are possible. Each internal atom lies within one of the layers (see Fig. 3). The layers have a flat, circular shape (ranging from the shape of a regular hexagon to a circle). The layers are concentrically stacked on top of each other and form a symmetric l -stepped pyramid with a flat top (the plane of the layers is always parallel to the substrate plane). Atoms within each layer are in the same plane, with only edge atoms displaced downwards, smoothing the stepped shape of the pyramid. Atoms Ar, Kr, and Xe

TABLE IV: Dependence on the number of encapsulated krypton atoms N_g and the number of layers l of the relative specific energy ΔE , pressure P , height H , radius R , and density d of the stationary state of the nanobubble.

N_g	l	ΔE (eV)	P (GPa)	H (Å)	R (Å)	d (g/cm ³)	H/R
188	1	0	1.442	3.35	27.46	3.02	0.122
	2	0.0234	1.509	5.99	25.78	2.86	0.232
260	1	0	1.357	3.35	32.23	3.11	0.084
	2	0.0179	1.389	6.45	28.48	2.96	0.226
398	1	0	1.284	3.35	39.91	3.17	0.084
	2	0.0086	1.240	6.53	33.90	3.05	0.193
614	1	0	1.194	3.36	49.24	3.26	0.068
	2	0.0041	1.133	6.52	40.75	3.13	0.160
	3	0.0145	1.151	9.07	39.78	3.06	0.228
962	1	0	1.131	3.35	61.63	3.30	0.054
	2	-0.0006	1.063	6.53	49.85	3.19	0.131
	3	0.0068	1.023	9.61	47.47	3.12	0.202
1335	1	0	1.098	3.35	72.43	3.35	0.046
	2	-0.0033	0.982	6.53	57.02	3.24	0.115
	3	0.0015	0.964	9.72	53.34	3.16	0.182
	4	0.0930	0.959	12.49	51.15	3.14	0.206
1828	1	0	1.069	3.35	84.72	3.37	0.040
	2	-0.0055	0.944	6.54	66.20	3.26	0.099
	3	-0.0029	0.892	9.70	60.17	3.20	0.161
	4	0.0005	0.941	12.41	60.66	3.17	0.205
2909	1	0	1.038	3.35	106.65	3.41	0.031
	2	-0.0080	0.872	6.54	81.66	3.31	0.080
	3	-0.0070	0.852	9.71	74.79	3.23	0.130
	4	-0.0047	0.813	12.94	71.05	3.19	0.182
	5	-0.0015	0.877	15.41	72.16	3.18	0.214
3936	1	0	1.018	3.36	123.73	3.44	0.027
	2	-0.0096	0.827	6.55	93.70	3.34	0.070
	3	-0.0094	0.806	9.71	85.27	3.25	0.114
	4	-0.0082	0.761	12.91	79.40	3.21	0.163
	5	-0.0061	0.796	15.98	78.45	3.20	0.204

differ in size, hence the interlayer distances for them are $\Delta h = 3.0, 3.2$, and 3.6 Å, respectively. For argon atoms, two- and three-layer structures at $N_g = 2463$ were first obtained in [34].

Covering the l -stepped pyramid from above with a graphene sheet is achieved through its local stretching. The valence bonds of the sheet stretch over the group of encapsulated atoms, while outside this zone the sheet remains in an undeformed state, lying flush against the substrate—see Fig. 4. The most significant stretching of C–C bonds occurs over the layer boundaries, where the deformation energy can reach values of 0.01 eV per carbon atom. As seen in Fig. 4, the zones of sheet stretching strictly correspond to the stepped structure of the pyra-

mid of encapsulated atoms. For example, for $N_g = 3936$ and l -layer states with $l = 1, 2, 3$, stretching of the sheet occurs only over the edges of the layers. For states with a larger number of layers ($l = 4, 5$), stretching occurs more uniformly across the entire surface of the nanobubble, but the maximum values are always reached at its base (over the edge of the first layer).

Local stretching of the valence bonds of the graphene sheet induces pressure p_n on the encapsulated atoms. As shown in Fig. 5, the pressure arising from encapsulation is localized only on the surface of the nanobubble. Over the layer boundaries, the pressure can reach maximum values of up to 10 GPa, while the average pressure value is $P \sim 1$ GPa. The highest pressure is experienced by single-layer packings of internal atoms. The average pressure value decreases with an increasing number of layers.

The maximum possible number of layers, l_m , depends on the number of internal atoms, N_g (l_m increases with increasing N_g). For argon atoms, only single-layer packings ($l_m = 1$) are possible for $N_g \leq 150$, while for $150 < N_g < 900$, single- and double-layer packings ($l_m = 2$) are possible. For $900 < N_g < 1800$, the maximum number of layers is $l_m = 3$; for $1800 < N_g < 2800$, it is $l_m = 4$; and for $2800 < N_g < 4000$, it is $l_m = 5$. A single-layer packing exists for any number of atoms. Therefore, the relative energy of a stationary state can be measured from the energy of the single-layer packing: $\Delta E = (E_l - E_1)/N_g$, where E_l is the energy of the l -layer stationary state.

The dependence of the relative specific energy ΔE , internal pressure P , height H , radius R , and density d of the nanobubble's stationary state on the number of argon atoms N_g is given in Table III. As can be seen from the table, single-layer stationary states are the most energetically favorable for $N_g < 900$. For $900 < N_g < 3000$, two-layer states become more favorable, and for $N_g > 3000$, three- and four-layer states are more favorable. The pressure inside the encapsulation monotonically decreases with an increasing number of atoms. With an increasing number of layers, a slight decrease in pressure and density is observed. The height of the nanobubble, H , always takes a discrete set of values proportional to the number of layers l : $H \approx h_0 + (l - 1)\Delta h$.

For krypton atoms, the dependence of ΔE , P , H , R , and d on the number of internal atoms N_g is presented in Table IV. Here, for $N_g \leq 140$, the maximum number of layers is $l_m = 1$; for $140 < N_g < 600$, $l_m = 2$; for $600 < N_g < 1300$, $l_m = 3$; for $1300 < N_g < 2800$, $l_m = 4$; and for $2800 < N_g < 4000$, $l_m = 5$. As can be seen from the table, single-layer stationary states are the most energetically favorable for $N_g < 900$, while two-layer states are favorable for $900 < N_g < 4000$. Here too, the pressure inside the nanobubble monotonically decreases with an increasing number of atoms. Pressure and density reach their maximum values for single-layer states.

For xenon atoms, the dependence of ΔE , P , H , R ,

TABLE V: Dependence on the number of encapsulated xenon atoms N_g and the number of layers l of the relative specific energy ΔE , pressure P , height H , radius R , and density d of the stationary state of the nanobubble.

N_g	l	ΔE (eV)	P (GPa)	H (Å)	R (Å)	d (g/cm ³)	H/R
188	1	0	1.476	3.57	31.54	3.52	0.113
	2	0.0278	1.492	6.87	28.87	3.28	0.231
260	1	0	1.361	3.58	36.85	3.60	0.097
	2	0.0216	1.367	7.15	32.62	3.34	0.219
398	1	0	1.296	3.58	45.58	3.66	0.079
	2	0.0061	1.096	7.21	38.37	3.45	0.188
614	1	0	1.227	3.59	56.15	3.75	0.064
	2	-0.0009	1.133	7.23	45.86	3.50	0.158
	3	0.0108	1.165	10.36	44.91	3.41	0.213
962	1	0	1.180	3.58	70.11	3.80	0.051
	2	-0.0068	1.083	7.23	56.27	3.55	0.128
	3	-0.0013	1.015	10.76	53.26	3.45	0.202
1335	1	0	1.146	3.58	82.44	3.84	0.043
	2	-0.0117	1.006	7.24	65.08	3.57	0.111
	3	-0.0104	0.965	10.88	60.08	3.49	0.181
	4	0.0012	0.980	14.04	58.02	3.45	0.242
1828	1	0	1.125	3.59	96.27	3.86	0.037
	2	-0.0160	0.953	7.25	74.47	3.62	0.097
	3	-0.0306	0.880	10.93	67.94	3.51	0.161
	4	-0.0124	0.925	14.36	65.59	3.48	0.219
2909	1	0	1.090	3.60	120.99	3.90	0.030
	2	-0.0198	0.897	7.27	92.58	3.65	0.079
	3	-0.0238	0.860	10.89	83.19	3.55	0.131
	4	-0.0228	0.841	14.55	79.27	3.50	0.184
	5	-0.0171	0.846	17.81	76.76	3.47	0.232
3936	1	0	1.077	3.60	140.68	3.91	0.026
	2	-0.0218	0.872	7.26	106.36	3.67	0.068
	3	-0.0272	0.828	10.88	95.06	3.56	0.114
	4	-0.0286	0.791	14.53	87.11	3.52	0.167
	5	-0.0255	0.794	17.79	88.19	3.47	0.202
	6	-0.0233	0.804	20.81	85.72	3.48	0.243

and d on N_g is presented in Table V. Here, for $N_g \leq 116$, the maximum number of layers is $l_m = 1$; for $116 < N_g < 600$, $l_m = 2$; for $600 < N_g < 1300$, $l_m = 3$; for $1300 < N_g < 2800$, $l_m = 4$; for $2800 < N_g < 3800$, $l_m = 5$; and for $3800 < N_g < 4000$, $l_m = 6$. As can be seen from the table, single-layer stationary states are the most energetically favorable for $N_g < 600$, two-layer states are favorable for $600 < N_g < 1400$, and three-layer states are favorable thereafter. Here too, the pressure inside the nanobubble monotonically decreases with an increasing number of atoms, and pressure and density reach their maximum values for single-layer packings.

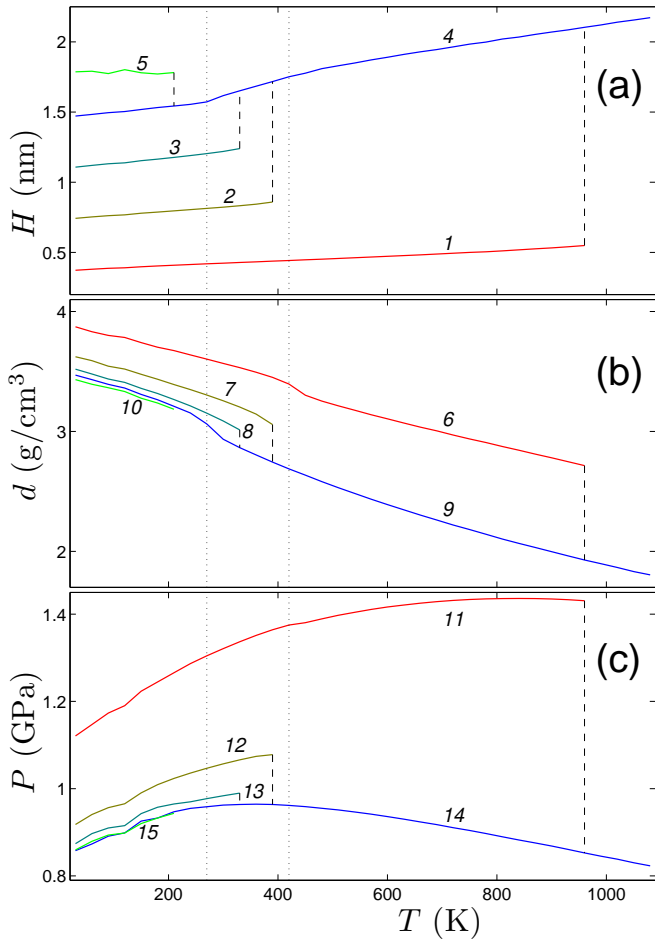


FIG. 6: Dependence on temperature T of (a) height H , (b) density d , and (c) internal pressure P for a graphene nanobubble with $N_g = 2909$ xenon atoms. Curves 1, 6, 11 correspond to the state with $l = 1$; curves 2, 7, 12 – to $l = 2$, ..., and curves 5, 10, 15 – to $l = 5$ layers. The dashed vertical lines correspond to the transition temperatures between states $l \rightarrow 4$: $T_1 = 960$, $T_2 = 390$, $T_3 = 330$, and $T_5 = 210$ K. The dotted vertical lines correspond to the melting temperature of the single-layer (420 K) and four-layer state (270 K).

IV. STABILITY OF STATIONARY STATES TO THERMAL FLUCTUATIONS

Note that all stationary states of nanobubbles obtained by solving the energy minimization problem are always stable. To verify their stability against thermal fluctuations, we performed simulations of nanobubble dynamics at temperatures $T \leq 1080$ K.

Dynamics of a thermalized graphene sheet with encapsulated atoms is described by the system of Langevin equations:

$$M_n \ddot{\mathbf{u}}_n = -\frac{\partial H}{\partial \mathbf{u}_n} - \Gamma M_n \dot{\mathbf{u}}_n + \Xi_n, \quad n = 1, \dots, N, \quad (13)$$

where the mass $M_n = M_c$ for $n = 1, \dots, N_c$ and $M_n = M_g$

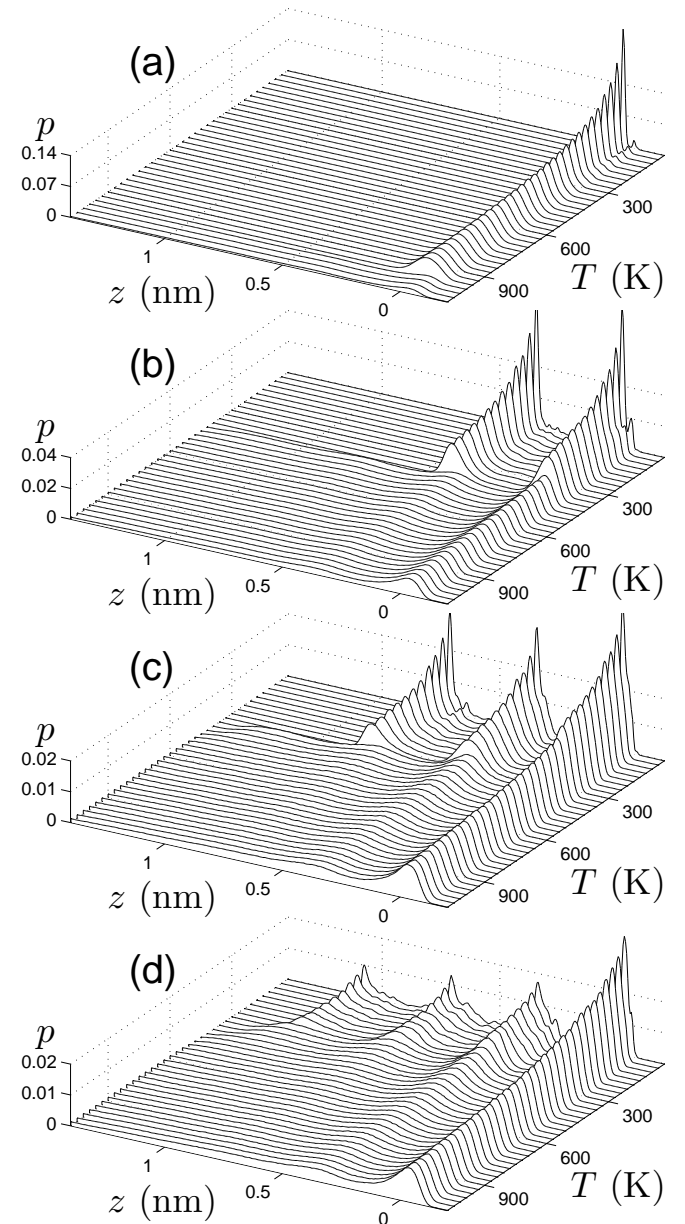


FIG. 7: Dependence on temperature T of the vertical displacement distribution $p(z)$ for l -layer states of $N_g = 2909$ internal xenon atoms: (a) $l = 1$; (b) $l = 2$; (c) $l = 3$; and (d) $l = 4$.

for $n = N_c + 1, \dots, N$ (the total number of atoms is $N = N_c + N_g$). Here, $\Gamma = 1/t_r$ is the friction coefficient characterizing the intensity of energy exchange with the thermostat (relaxation time $t_r = 10$ ps), and $\Xi_n = \{\xi_{n,i}\}_{i=1}^3$ is a three-dimensional vector of normally distributed random forces normalized by the following conditions:

$$\langle \xi_{n,i}(t) \xi_{k,j}(s) \rangle = 2\Gamma M_n k_B T \delta_{nk} \delta_{ij} \delta(t-s).$$

Here, T is the thermostat temperature and k_B is the Boltzmann constant.

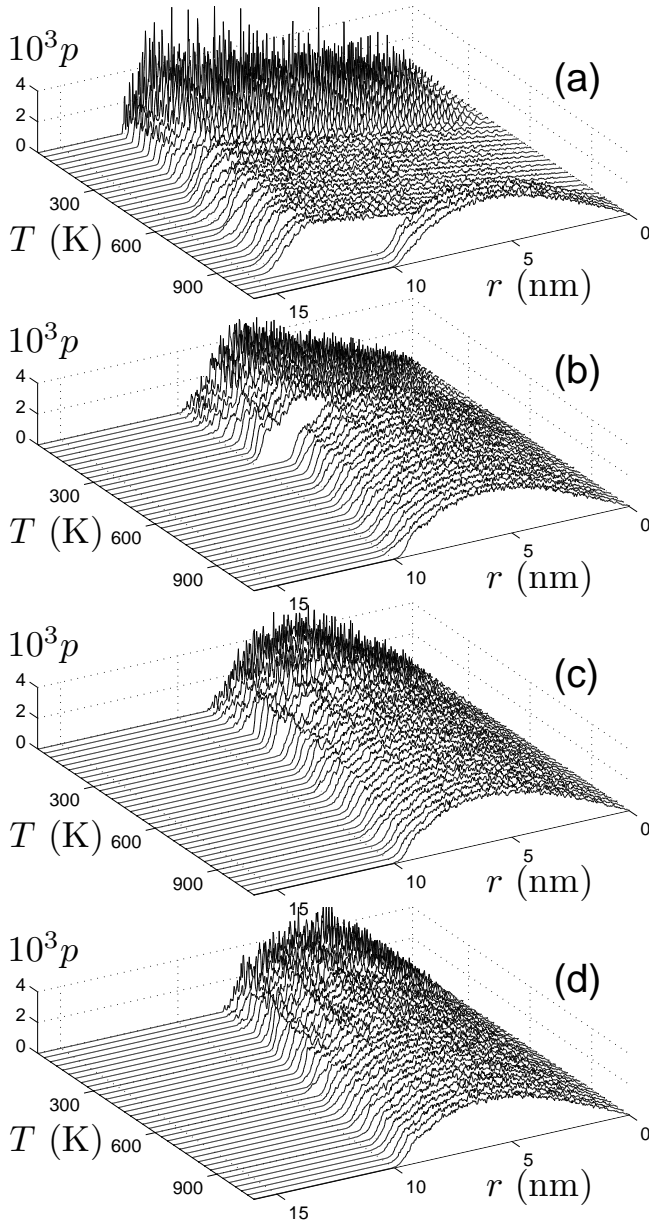


FIG. 8: Temperature dependence T of the transverse displacement distribution $p(r)$ from the center of mass for l -layer states of $N_g = 2909$ inner xenon atoms: (a) $l = 1$; (b) $l = 2$; (c) $l = 3$; and (d) $l = 4$.

The relaxation time t_r determines the intensity of energy exchange with the thermostat. In the simulated molecular system, the role of the thermostat is played by a flat substrate, to which the atoms are weakly coupled via non-valence interactions. For such interactions, the relaxation time is typically $t_r \sim 100$ ps. For the convenience of numerical simulation, we use a smaller value, $t_r = 10$ ps. This allows us to significantly reduce the numerical integration time required to reach an equilibrium state and obtain reliable averages.

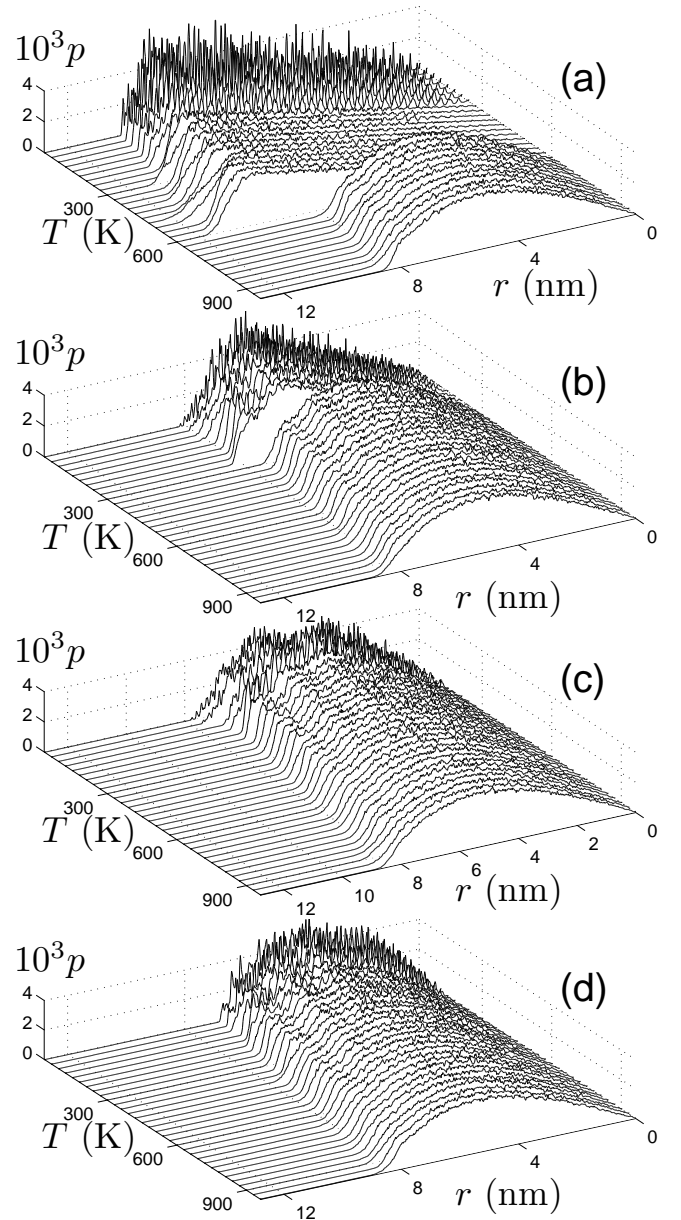


FIG. 9: Temperature dependence T of the transverse displacement distribution $p(r)$ from the center of mass for l -layer states of $N_g = 2909$ inner argon atoms: (a) $l = 1$; (b) $l = 2$; (c) $l = 3$; and (d) $l = 4$.

We numerically integrate the system of equations of motion (13) with initial conditions corresponding to a stationary nanobubble state:

$$\{\mathbf{u}_n(0) = \mathbf{u}_n^0, \dot{\mathbf{u}}_n(0) = 0\}_{n=1}^N. \quad (14)$$

The equations of motion Eq. (13) with initial conditions (14) are solved numerically using the velocity Verlet method [55]. A time step of 1 fs is used in the simulations, as further reduction of the time step has no appreciable effect on the results.

Numerical simulations of the dynamics showed that among the l -layer states of the nanobubble, there is always one "ground" state, which smoothly transitions into a layerless liquid state as the temperature increases. All other states transition into this ground state at a specific temperature. The dependence of the nanobubble's height H , density d , and internal pressure P on temperature is shown in Fig. 6.

As can be seen from the figure, for a bubble with $N_g = 2909$ xenon atoms, a single-layer packing ($l = 1$) persists up to a very high temperature $T_1 = 960$ K. Further temperature increase leads to its transition into a layerless molten state, accompanied by a sharp increase in height H , a decrease in density d , and internal pressure P . Two-layer atom packings ($l = 2$) persist up to a temperature $T_2 = 390$ K, at which they transition into a four-layer packing. This transition is also accompanied by a sharp increase in height and a decrease in density. Three-layer packings ($l = 3$) persist up to a temperature $T_3 = 330$ K, and five-layer packings ($l = 5$) persist up to $T_5 = 210$ K. Here, the ground state is the four-layer ($l = 4$) packing. A similar pattern occurs for argon and krypton atoms: for Ar, the transition temperatures are $T_l = 600, 270, 180, 30$ K; for Kr— $T_l = 750, 360, 240, 150$ K, where $l = 1, 2, 3, 5$.

In Tables III, IV, V, the rows corresponding to the ground states are given in italics. Note that the ground states are not always the most energetically favorable. Their key feature is the smooth (non-abrupt) change in their shape with increasing temperature.

Conformational changes of the encapsulated atom cluster are reflected in the change in the distribution of atoms by their vertical $\{z_n\}_{n=N_c}^N$ (Fig. 7) and radial (in-plane) displacements from the center of mass:

$$\{r_n = [(x_n - x_c)^2 + (y_n - y_c)^2]^{1/2}\}_{n=N_c+1}^N$$

(Figs. 8, 9).

As can be seen from Fig. 7 (a, b, c), the shape of the vertical displacement distribution changes sharply at the temperature of l -layer state stability loss. For $l \neq 4$, the clearly pronounced layered structure of the cluster disappears here. For the ground state ($l = 4$), only a gradual, smooth broadening of the layered structure occurs with increasing temperature, with only the first layer of atoms adjacent to the substrate remaining clearly pronounced—see Fig. 7 (d).

Radial displacements also show changes in the distribution shape at the transition temperature T_l . The transition to a state with a larger number of layers leads to a sharp decrease in the diameter of the inner atom cluster—see Figs. 8 (a, b, c) and 9 (a, b, c). For the ground state with $l = 4$ layers, only a continuous, gradual increase in the cluster diameter (its thermal expansion) occurs—see Figs. 8 (d) and 9 (d).

The shape of the radial distribution also allows one to judge the phase state of the cluster. At low temperature, the radial distribution has a discrete structure characteristic of a crystalline (solid) state. Upon reaching the

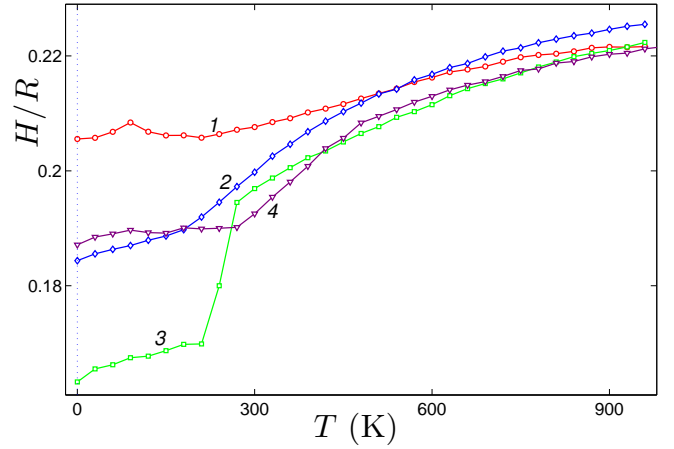


FIG. 10: Temperature dependence T of the ratio H/R for the ground state of the nanobubble: with $N_g = 962$ and 2909 argon atoms (curves 1 and 2); with $N_g = 3936$ krypton atoms (curve 3); with $N_g = 2909$ xenon atoms (curve 4).

melting temperature $T_{l,m}$, the discrete distribution shape is replaced by a continuous one, characteristic of a liquid state. For $N_g = 2909$ xenon atoms, the melting of the single-layer cluster occurs at $T_{1,m} = 420 \div 450$ K, and of the four-layer cluster at $T_{4,m} = 270 \div 300$ K—see Fig. 8. For argon atoms, the melting temperatures are $T_{1,m} = 240 \div 270$ K, $T_{4,m} = 150 \div 180$ K (see Fig. 9), and for krypton $T_{1,m} = 300 \div 330$ K, $T_{4,m} = 210 \div 240$ K. Such high melting temperatures are explained by the high value of internal pressure—see Fig. 6 (c).

The existence of several stable states with different numbers of atom layers l at low temperatures indicates that the nanobubbles here cannot have a universal (scalable) shape, and the height-to-radius ratio is not constant. Indeed, for a single-layer state ($l = 1$), increasing the number of internal atoms N_g does not change the nanobubble's height ($H \approx 3.3$ Å, while its radius R grows as $\sqrt{N_g}$; therefore, the ratio $H/R \rightarrow 0$ as $N_g \rightarrow \infty$). Based on the data in Tables III, IV, and V, the ratio H/R can vary from 0 to 0.24 here. The violation of the scaling rule for graphene bubbles with a radius of ~ 1 nm was noted in the experimental study [24], where they were created via the implantation of noble gas ions He, Ne, and Ar. As can be seen from the table data, the relation $H/R \approx 0.2$ holds only for the ground states of the nanobubble.

The dependence of the ratio H/R on temperature T for the ground states of the nanobubble is shown in Fig. 10. As can be seen from the figure, the value of H/R increases monotonically with temperature, while the spread of values decreases: H/R varies within the intervals $[0.163, 0.206]$ at $T = 0$ K; $[0.192, 0.208]$ at $T = 300$ K; $[0.211, 0.217]$ at $T = 600$ K. These estimates are in good agreement with the universal value $H/R = 0.204$ obtained in [36] for a graphene nanobubble with an ideal gas. Note that the study [37] reported an estimate of $H/R \approx 0.13$

for graphene nanobubbles with argon atoms at $T = 2$ K, indicating that the simulation used not a ground stationary state of the nanobubble, but rather a state with a smaller number of layers.

V. CONCLUSION

Using the example of inert gas atoms (Ar, Kr, Xe), it has been shown that graphene nanobubbles located on flat substrates are multistable systems. A nanobubble can have many stable stationary states, each characterized by the number of layers l in the internal atom cluster. Inside the nanobubble, each atom lies within one of the layers. The layers have a circular, flat shape, are concentrically stacked on top of each other, and form an l -stepped pyramid with a flat top. Atoms within each layer lie in a single plane, with only the edge atoms displaced downwards, smoothing the stepped shape of the pyramid. The covering of the pyramid from above by a graphene sheet occurs due to its local stretching. The sheet's valence bonds are stretched only above the group of encapsulated atoms; outside this coverage zone, the sheet remains undeformed and tightly adheres to the substrate. The strongest stretching (up to one percent) occurs above the edges of the layers.

The maximum possible number of layers l_m increases monotonically with the number of internal atoms N_g . For argon atoms, only single-layer stationary states ($l_m = 1$) are possible for $N_g \leq 150$; for $150 < N_g < 900$ —single-layer and double-layer states ($l_m = 2$); for $900 < N_g <$

1800, $l_m = 3$; for $1800 < N_g < 2800$, $l_m = 4$; and for $2800 < N_g < 4000$, $l_m = 5$. The graphene sheet, due to van der Waals interaction with the substrate, presses the cluster of encapsulated atoms to substrate, creating pressures $P \sim 1$ GPa. The highest pressure is experienced by single-layer packings of internal atoms. The magnitude of the pressure decreases as the number of layers increases.

Thermal fluctuation modeling shows that among all l -layer states of the nanobubble, there is always one "ground" state, which smoothly transitions into a layerless liquid state as the temperature increases. The other states transition into this state at a specific temperature T_l . For example, for $N_g = 2909$ encapsulated atoms, the ground state is the four-layer packing ($l = 4$). For Xe atoms, the l -layer states persist up to temperatures $T_l = 960, 390, 330, 210$ K; for Ar atoms, $T_l = 600, 270, 180, 30$ K; and for Kr atoms—750, 360, 240, 150 K, where $l = 1, 2, 3, 5$.

The existence of several stable states with different numbers of layers in the internal atom cluster at low temperatures indicates that universal scaling does not hold for these nanobubbles. The height-to-radius ratio H/R of the nanobubble is not constant and can vary from 0 to 0.24. The universal relation $H/R \approx 0.2$ holds only for the ground states.

Acknowledgements

The research was funded by the Russian Science Foundation (RSF) (project No. 25-73-20038).

[1] K. S. Novoselov, A. K. Geim, S. V. Morozov, D. Jiang, Y. Zhang, S. V. Dubonos, I. V. Grigorieva, A. A. Firsov. Electric Field Effect in Atomically Thin Carbon Films. *Science* **306**(5696), 666-669 (2004). <https://doi.org/10.1126/science.1102896>

[2] A. K. Geim, K. S. Novoselov. The rise of graphene. *Nat. Mater.* **6**(3), 183-191 (2007). <https://doi.org/10.1038/nmat1849>

[3] C. Soldano, A. Mahmood, E. Dujardin. Production, Properties and Potential of Graphene. *Carbon* **48**(8), 2127-2150 (2010). <https://doi.org/10.1016/j.carbon.2010.01.058>

[4] J. A. Baimova, B. Liu, S. V. Dmitriev, K. Zhou. Mechanical properties and structures of bulk nanomaterials based on carbon nanopolymorphs. *Phys. Status Solidi RRL* **8**(4), 336-340 (2014). <https://doi.org/10.1002/pssr.201409063>

[5] J. A. Baimova, E. A. Korznikova, S. V. Dmitriev, B. Liu and K. Zhou. Review on crumpled graphene: Unique mechanical properties. *Rev. Adv. Mater. Sci.* **39**, 69-83 (2014). https://www.ipme.ru/e-journals/RAMS/no.13914/11_13914_baimova.pdf

[6] A. K. Geim. Graphene: status and prospects. *Science* **324**(5934), 1530-1534 (2009). <https://doi.org/10.1126/science.1158877>

[7] C. Lee, X. Wei, J.W. Kysar, J. Hone. Measurement of the elastic properties and intrinsic strength of monolayer graphene. *Science* **321**(5887), 385-388 (2008). <https://doi.org/10.1126/science.1157996>

[8] A. A. Balandin, S. Ghosh, W. Bao, I. Calizo, D. Teweldebrhan, F. Miao, C. N. Lau. Superior thermal conductivity of single-layer graphene. *Nano Lett.* **8**(3), 902-907 (2008). <https://doi.org/10.1021/nl0731872>

[9] Y. Liu, C. Hu, J. Huang, B. G. Sumpter, R. Qiao. Tuning interfacial thermal conductance of graphene embedded in soft materials by vacancy defects. *J. Chem. Phys.* **142**(24), 244703 (2015). <https://doi.org/10.1063/1.4922775>

[10] A. K. Geim and I. V. Grigorieva. Van der Waals heterostructures. *Nature* **499**, 419-425 (2013). <https://doi.org/10.1038/nature12385>

[11] L. Wang, I. Meric, P.Y. Huang, Q. Gao, Y. Gao, H. Tran, T. Taniguchi, K. Watanabe, L.M. Campos, D. A. Muller, J. Guo, P. Kim, J. Hone, K.L. Shepard, and C.R. Dean. One-dimensional electrical contact to a two-dimensional material. *Science* **342**, 614-617 (2013). <https://doi.org/10.1126/science.1244358>

[12] R. Xiang, T. Inoue, Y. Zheng, A. Kumamoto, Y. Qian, Y. Sato, M. Liu, D. Tang, D. Gokhale, J. Guo, K. Hisama, S. Yotsumoto, T. Ogamoto, H. Arai, Y. Kobayashi, H.

Zhang, B. Hou, A. Anisimov, M. Maruyama, Y. Miyata, S. Okada, S. Chiashi, Y. Li, J. Kong, E.I. Kauppinen, Y. Ikuhara, K. Suenaga, S. Maruyama. One-dimensional van der Waals heterostructures. *Science* **367**, 537-542 (2020). <https://doi.org/10.1126/science.aaz2570>

[13] Y. Zhang, C. Hu, B. Lyu, H. Li, Z. Ying, L. Wang, A. Deng, X. Luo, Q. Gao, J. Chen, J. Du, P. Shen, K. Watanabe, T. Taniguchi, J.-H. Kang, F. Wang, Y. Zhang, and Z. Shi. Tunable cherenkov radiation of phonon polaritons in silver nanowire/hexagonal boron nitride heterostructures. *Nano Lett.* **20**, 2770-2777 (2020). <https://doi.org/10.1021/acs.nanolett.0c00419>

[14] K.S. Vasu, E. Prestat, J. Abraham, J. Dix, R.J. Kashtiban, J. Beheshtian, J. Sloan, P. Carbone, M. Neek-Amal, S.J. Haigh, A.K. Geim, and R.R. Nair. Van der Waals pressure and its effect on trapped interlayer molecules. *Nat. Commun.* **7**, 12168 (2016). <https://doi.org/10.1038/ncomms12168>

[15] E. Khestanova, F. Guinea, L. Fumagalli, A.K. Geim, and I.V. Grigorieva. Universal shape and pressure inside bubbles appearing in van der Waals heterostructures. *Nat. Commun.* **7**, 12587 (2016). <https://doi.org/10.1038/ncomms12587>

[16] C. Hu, J. Chen, X. Zhou, Y. Xie, X. Huang, Z. Wu, S. Ma, Z. Zhang, K. Xu, N. Wan, Y. Zhang, Q. Liang, and Z. Shi. Collapse of carbon nanotubes due to local high-pressure from van der Waals encapsulation. *Nat. Commun.* **15**, 3486 (2024). <https://doi.org/10.1038/s41467-024-47903-3>

[17] L. Zhang, Y. Wang, J. Lv, and Y. Ma. Materials Discovery at High Pressures. *Nature Reviews Materials*, **2**, 17005 (2017). <https://doi.org/10.1038/natrevmats.2017.5>

[18] J. Zheng, X. Liu, P. Xu, P. Liu, Y. Zhao, and J. Yang. Development of high pressure gaseous hydrogen storage technologies. *International Journal of Hydrogen Energy*, **37**(1), 1048-1057 (2012). <https://doi.org/10.1016/j.ijhydene.2011.02.125>

[19] M. M. Slepchenkov, P. V. Barkov and O. E. Glukhova. High-Density Hydrogen Storage in a 2D-Matrix from Graphene Nanoblisters: A Prospective Nanomaterial for Environmentally Friendly Technologies. *Crystals*, **8**(4), 161 (2018). <https://doi.org/10.3390/cryst8040161>

[20] N.G. Apkadirova, K.A. Krylova, J.A. Baimova. Effect of external pressure on the hydrogen storage capacity of a graphene flake: molecular dynamics. *Lett. Mater.*, **12**(4s), 445-450 (2022). <https://doi.org/10.22226/2410-3535-2022-4-445-450>

[21] D. A. Sanchez, Z. Dai, P. Wang, A. Cantu-Chavez, C. J. Brennan, R. Huang and N. Lu. Mechanics of spontaneously formed nanoblisters trapped by transferred 2D crystals. *Proceedings of the National Academy of Sciences*, **115**(31), 7884-7889 (2018). <https://doi.org/10.1073/pnas.1801551115>

[22] E. Blundo, C. Di Giorgio, G. Pettinari, T. Yildirim, M. Felici, Y. Lu, F. Bobba and A. Polimeni. Engineered Creation of Periodic Giant, Nonuniform Strains in MoS₂ Monolayers. *Advanced Materials Interfaces*, **7**(17), 2000621 (2020). <https://doi.org/10.1002/admi.202000621>

[23] G. Zamborlini, M. Imam, L. L. Patera, T. O. Mentes, N. Stojic, C. Africh, A. Sala, N. Binggeli, G. Comelli and A. Locatelli, Nanobubbles at GPa pressure under graphene. *Nano Lett.*, **15**, 6162-6169 (2015). <https://doi.org/10.1021/acs.nanolett.5b02475>

[24] R. Villarreal, P.-C. Lin, F. Faraji, N. Hassani, H. Bana, Z. Zarkua, M. N. Nair, H.-C. Tsai, M. Auge, F. Junge, H. C. Hofsass, S. De Gendt, S. De Feyter, S. Brems, E. H. Ahlgren, E. C. Neyts, L. Covaci, F. M. Peeters, M. Neek-Amal, and L. M. C. Pereira. Breakdown of Universal Scaling for Nanometer-Sized Bubbles in Graphene. *Nano Lett.*, **21**, 8103-8110 (2021). <https://doi.org/10.1021/acs.nanolett.1c02470>

[25] K. M. Zahra, C. Byrne, A. Alieva, C. Casiraghi and A. S. Walton. Intercalation, decomposition, entrapment - a new route to graphene nanobubbles. *Phys. Chem. Chem. Phys.* **22**(14), 7606-7615 (2020). <https://doi.org/10.1039/d0cp00592d>

[26] K. Yue, W. Gao, R. Huang and K. M. Liechti. Analytical methods for the mechanics of graphene bubbles. *J. Appl. Phys.* **112**, 083512 (2012). <https://doi.org/10.1063/1.4759146>

[27] P. Wang, W. Gao, Z. Cao, K. M. Liechti and R. Huang. Numerical Analysis of Circular Graphene Bubbles. *Journal of Applied Mechanics*, **80**, 040905 (2013). <https://doi.org/10.1115/1.4024169>

[28] Z. Dai, Y. Hou, D. A. Sanchez, G. Wang, C. J. Brennan, Z. Zhang, L. Liu and N. Lu. Interface-Governed Deformation of Nanobubbles and Nanotents Formed by Two-Dimensional Materials. *Phys. Rev. Lett.*, **121**, 266101 (2018). <https://doi.org/10.1103/PhysRevLett.121.266101>

[29] P. Zhilyaev, E. Iakovlev and I. Akhatov. Liquid-gas phase transition of Ar inside graphene nanobubbles on the graphite. *Nanotechnology*, **30**(21), 215701 (2019). <https://doi.org/10.1088/1361-6528/ab061f>

[30] E. Iakovlev, P. Zhilyaev and I. Akhatov. Modeling of the phase transition inside graphene nanobubbles filled with ethane. *Phys. Chem. Chem. Phys.*, **21**, 18099-18104 (2019). <https://doi.org/10.1039/c9cp03461g>

[31] T. Aslyamov, E. Iakovlev, I. S. Akhatov and P. Zhilyaev. Model of graphene nanobubble: Combining classical density functional and elasticity theories. *J. Chem. Phys.* **152**, 054705 (2020). <https://doi.org/10.1063/1.5138687>

[32] Z.-X. Qu, B.-S. Wang, and J.-W. Jiang. The Gas in Graphene Bubbles: An Improved van der Waals Equation Description. *J. Phys. Chem. C*, **127**, 9205-9212 (2023). <https://doi.org/10.1021/acs.jpcc.2c08173>

[33] A. Lyublinskaya, S. Babkin and I. Burnistrov. Effect of anomalous elasticity on bubbles in van der Waals heterostructures. *Physical Review E*, **101**, 033005 (2020). <https://doi.org/10.1103/PhysRevE.101.033005>

[34] E. Iakovlev, P. Zhilyaev and I. Akhatov. Atomistic study of the solid state inside graphene nanobubbles. *Scientific reports*, **7**, 17906 (2017). <https://doi.org/10.1038/s41598-017-18226-9>

[35] H. Ghorbanfekr-Kalashami, K. Vasu, R. R. Nair, F. M. Peeters and M. Neek-Amal. Dependence of the shape of graphene nanobubbles on trapped substance. *Nature communications*, **8**, 1-11 (2017). <https://doi.org/10.1038/ncomms15844>

[36] S. K. Jain, V. Juricic, and G. T. Barkema. Probing the Shape of a Graphene Nanobubble. *Phys. Chem. Chem. Phys.*, **19**, 7465-7470 (2017). <https://doi.org/10.1039/C6CP08535K>

[37] M. Korneva and P. Zhilyaev. Solid-liquid phase transition inside Van der Waals nanobubbles: tomistic perspective. *Phys. Chem. Chem. Phys.*, **25**, 18788-18796 (2023).

https://doi.org/10.1039/D3CP01285A

[38] Z.-X. Qu and J.-W. Jiang. Nanobubble-induced significant reduction of the interfacial thermal conductance for few-layer graphene *Phys. Chem. Chem. Phys.*, **25**, 28651 (2023). <https://doi.org/10.1039/d3cp04085b>

[39] Z.-X. Qu, C.-X. Cui, J.-W. Jiang. Bubble-Induced Strong Thermal Contraction for Graphene. *ASME Journal of Heat and Mass Transfer*, **145**(12), 1-13 (2023). <https://doi.org/10.1115/1.4063230>

[40] A. V. Savin, Y. Kivshar, and B. Hu. Suppression of thermal conductivity in graphene nanoribbons with rough edges. *Phys. Rev. B*, **82**, 195422 (2010). <https://doi.org/10.1103/PhysRevB.82.195422>

[41] A. V. Savin and Yu. S. Kivshar. Discrete breathers in carbon nanotubes. *EPL* **82**(6), 66002 (2008). <https://doi.org/10.1209/0295-5075/82/66002>

[42] Z. H. Aitken, R. Huang. Effects of mismatch strain and substrate surface corrugation on morphology of supported monolayer graphene. *J. Appl. Phys.* **107**, 123531 (2010). <https://doi.org/10.1063/1.3437642>

[43] K. Zhang and M. Arroyo. Adhesion and friction control localized folding in supported graphene. *J. Appl. Phys.* **113**, 193501 (2013). <https://doi.org/10.1063/1.3437642>

[44] K. Zhang, M. Arroyo. Understanding and strain-engineering wrinkle networks in supported graphene through simulations. *Journal of the Mechanics and Physics of Solids* **72**, 61-74 (2014). <https://doi.org/10.1016/j.jmps.2014.07.012>

[45] S. P. Koenig, N. G. Boddeti, M. L. Dunn, J. S. Bunch. Ultrastrong adhesion of graphene membranes. *Nature Nanotech* **6**, 543-546 (2011). <https://doi.org/10.1038/nnano.2011.123>

[46] A. K. Rappe, C. J. Casewit, K. S. Colwell, W. A. Goddard III, W. M. Skiff. UFF, a Full Periodic Table Force Field for Molecular Mechanics and Molecular Dynamics Simulations. *J. Am. Chem. Soc.* **114**(25), 10024-10035 (1992). <https://doi.org/10.1021/ja00051a040>

[47] J. Vogt and S. Alvarez. van der Waals Radii of Noble Gases. *Inorg. Chem.* **53**(17), 9260-9266 (2014). <https://doi.org/10.1021/ic501364h>

[48] L. Lindsay and D. A. Broido. Optimized tersoff and brenner empirical potential parameters for lattice dynamics and phonon thermal transport in carbon nanotubes and graphene. *Phys. Rev. B* **81**, 205441 (2010). <https://doi.org/10.1103/PhysRevB.81.205441>

[49] S. J. Stuart, A. B. Tutein, J. A. Harrison. A reactive potential for hydrocarbons with intermolecular interactions. *J. Chem. Phys.* **112** (14), 6472-6486 (2000). <https://doi.org/10.1063/1.481208>

[50] D. W. Brenner, O. A. Shenderova, J. A. Harrison, S. J. Stuart, B. Ni, S. B. Sinnott. A second-generation reactive empirical bond order (rebo) potential energy expression for hydrocarbons, *J. Phys.: Condens. Matter*. **14** (4), 783-802 (2002). <https://doi.org/10.1088/0953-8984/14/4/312>

[51] S. G. Srinivasan, A. C. T. van Duin, P. Ganesh. Development of a reaxff potential for carbon condensed phases and its application to the thermal fragmentation of large fullerene. *J. Phys. Chem. A* **119**, 571-580 (2015). <https://doi.org/10.1021/jp510274e>

[52] I. V. Lebedeva, A. S. Minkin, A. M. Popov, A. A. Knizhnik. Elastic constants of graphene: Comparison of empirical potentials and dft calculations. *Phys. E* **108**, 326-338 (2019). <https://doi.org/10.1016/j.physe.2018.11.025>

[53] R. Fletcher and C. Reeves. Function Minimization by Conjugate Gradients. *Computer Journal* **7**(2), 149-154 (1964). <https://doi.org/10.1093/comjnl/7.2.149>

[54] D. F. Shanno, K. H. Phua. Algorithm 500: Minimization of Unconstrained Multivariate Functions [E4]. *ACM Transactions on Mathematical Software* **2**(1), 87-94 (1976). <https://doi.org/10.1145/355666.355673>

[55] L. Verlet. Computer "Experiments" on Classical Fluids. I. Thermodynamical Properties of Lennard-Jones Molecules. *Phys. Rev.* **159**, 98 (1967). <https://doi.org/10.1103/PhysRev.159.98>